Journal of Biomedical Optics

BiomedicalOptics.SPIEDigitalLibrary.org

In vivo imaging of melanoma-implanted magnetic nanoparticles using contrast-enhanced magneto-motive optical Doppler tomography

Ruchire Eranga Wijesinghe
Kibeom Park
Dong-Hyeon Kim
Mansik Jeon
Jeehyun Kim

SPIE.

Ruchire Eranga Wijesinghe, Kibeom Park, Dong-Hyeon Kim, Mansik Jeon, Jeehyun Kim, "*In vivo* imaging of melanoma-implanted magnetic nanoparticles using contrast-enhanced magneto-motive optical Doppler tomography," *J. Biomed. Opt.* **21**(6), 064001 (2016), doi: 10.1117/1.JBO.21.6.064001.

In vivo imaging of melanoma-implanted magnetic nanoparticles using contrast-enhanced magneto-motive optical Doppler tomography

Ruchire Eranga Wijesinghe,[a] Kibeom Park,[a] Dong-Hyeon Kim,[b,*] Mansik Jeon,[a,*] and Jeehyun Kim[a]
[a]Kyungpook National University, School of Electronics Engineering, College of IT Engineering, 80 Daehak-ro, Buk-gu, Daegu 41566, Republic of Korea
[b]3D Convergence Technology Center, 70 Dongnae-ro, Daegu 41061, Republic of Korea

Abstract. We conducted an initial feasibility study using real-time magneto-motive optical Doppler tomography (MM-ODT) with enhanced contrast to investigate the detection of superparamagnetic iron oxide (SPIO) magnetic nanoparticles implanted into *in vivo* melanoma tissue. The MM-ODT signals were detected owing to the phase shift of the implanted magnetic nanoparticles, which occurred due to the action of an applied magnetic field. An amplifier circuit-based solenoid was utilized for generating high-intensity oscillating magnetic fields. The MM-ODT system was confirmed as an effective *in vivo* imaging method for detecting melanoma tissue, with the performance comparable to those of conventional optical coherence tomography and optical Doppler tomography methods. Moreover, the optimal values of the SPIO nanoparticles concentration and solenoid voltage for obtaining the uppermost Doppler velocity were derived as well. To improve the signal processing speed for real-time imaging, we adopted multithread programming techniques and optimized the signal path. The results suggest that this imaging modality can be used as a powerful tool to identify the intracellular and extracellular SPIO nanoparticles in melanoma tissues *in vivo*. [DOI: 10.1117/1.JBO.21.6.064001]

Keywords: magneto-motive optical Doppler tomography; optical Doppler tomography; SD-optical coherence tomography; melanoma; superparamagnetic iron oxide; nanoparticles.

Paper 160033SSRR received Jan. 20, 2016; accepted for publication Jun. 1, 2016; published online Jun. 21, 2016.

1 Introduction

Biophotonics research for detecting melanoma cells in a clinical setting has been limited by either the resolution of the existing *in vivo* imaging techniques or the time required for performing histological analysis. In addition, rigorous detection of melanoma remains one of the most challenging problems in clinical dermatology.[1,2] Over the past few years, an increasing number of researchers have devoted attention to develop methods for visualizing melanoma cells. The most commonly used approaches are ultrasonography, fluorescein angiography, and color Doppler testing.[3,4] However, because these approaches require qualified experts, they are plagued by problems such as insufficiency or inadequacy of the retrieved material, delays in diagnosis, a lack of spatial resolution, and high cost.[5] All of these limitations have been known for a long time, and, to address them, alternative noninvasive methods of investigation have been vigorously pursued. Therefore, there is a great need for cost-effective and noninvasive methods that would allow resolving melanoma cells with sufficient clarity and contrast.

Optical coherence tomography (OCT) is a powerful noninvasive method, extensively used for imaging in ophthalmology,[6–8] dermatology,[9] dentistry,[10] and otolaryngology.[11] Moreover, optical Doppler tomography (ODT) is a functional extension of OCT that was developed for noninvasive imaging of blood or liquid flow.[12–14] The exceptional transverse resolution of ODT allows visualizing structures close to the cellular level, and its high-velocity sensitivity enables imaging of microcirculation in blood vessels to be resolved by conventional Doppler ultrasound methods.[15] To date, several extensions of ODT have been considered for monitoring changes in the vascular microstructure and fine structure of living tissues.[16,17] An implementation of phase-resolved ODT for the analysis of the blood flow velocity distributions in tissues has been reported; the analysis was derived from the Hilbert transformation of the interference signal.[18,19]

The interest in the development of contrast agents and contrast mechanisms appropriate to use as molecular contrast agents in OCT and ODT has become a prominent concern recently. In particular, the *in vivo* contrast within a sample can be dramatically improved owing to the significant scattering efficiency of contrast agents.[20] Subsequently, nanoparticles of various shapes and sizes can be synthesized to suit specific needs of biomedical therapy and imaging.[21,22] Hence, OCT and ODT have been recently combined with supplementary techniques for imaging cells and tissues containing superparamagnetic iron oxide (SPIO) magnetic nanoparticles. In various fields of medical imaging, human melanoma cells have been efficiently labeled using SPIO contrast agents. Since, it has been scientifically proved that SPIO nanoparticles are able to attach them to melanoma cells and the basic concept for this was obtained from magnetic hyperthermia studies. The magnetic nanoparticles can transform electromagnetic energy from an external high-frequency field to heat. As a consequence, if magnetic nanoparticles are put inside a melanoma and the whole objective sample is placed in an alternating magnetic field of well-chosen

*Address all correspondence to: Dong-Hyeon Kim, E-mail: andrew@knu.ac.kr; Mansik Jeon, E-mail: msjeon@knu.ac.kr.

1083-3668/2016/$25.00 © 2016 SPIE

amplitude and frequency, the melanoma cell temperature increases significantly compared to normal cells. The elevation of temperature may enhance melanoma oxygenation and radio- and chemosensitivity, which leads to an existence of a certain ratio of oxide. The amino-polyvinyl alcohol (PVA) coating of SPIO nanoparticles has a strong interaction to the oxides. Thus, the interaction with melanoma cells was dependent on the amino-PVA to iron oxide ratio and was an active mechanism displayed by melanoma cells compared to normal cells.[23–28] Moreover, for enhanced-contrast imaging of cells, magneto-motive optical coherence tomography (MM-OCT) and magneto-motive optical Doppler tomography (MM-ODT) were performed by using electromagnets, which modulated magnetic fields within the cells during OCT and ODT imaging.[29–32] On the other hand, it is well known that MM-OCT was first performed in a cell scaffold containing a mixture of microparticles-labeled and unlabeled macrophage cells,[32] while MM-ODT was first introduced for analyzing the contrast between red blood cells and hemoglobin.[33]

In this study, we performed initial feasibility experiments to validate the versatility along with the most optimal experimental conditions of MM-ODT for detecting magnetic nanoparticles implanted into melanoma tissue. Therefore, an extension of the MM-ODT approach was facilitated by optimizing the system performance for achieving a real-time comprehensive identification of nanoparticles implanted into *in vivo* and *ex vivo* samples. To the best of our knowledge, this is the first *in vivo* demonstration of melanoma tissue imaging in real time by using an MM-ODT system. The proposed method provides a powerful means to the clinical field, and thus is likely to improve the ability to detect melanoma in clinical settings.

2 Materials and Methods

2.1 *Magneto-Motive Optical Doppler Tomography System Description*

A typical spectrometer-based MM-ODT system is shown in Fig. 1 along with the experimental setup. The broadband light source in this study was a super-luminescent diode (SLD-35-HP, Superlum, Ltd.) with a center wavelength of 870 nm and a 3-dB bandwidth of 65 nm. The incident light beam from the laser source was split evenly by using a 50:50 optical fiber coupler into a reference path and a sample arm. A galvanometer-based optical scanner was integrated for transverse scanning of the sample arm and it was driven at a frequency of 56 Hz. To obtain optimal results and to minimize the saturated power owing to the backscattered beams, the imaging axis was not maintained coaxially with the magnetic field gradient. Further, Fig. 1 shows the schematic of a solenoid with a core that generated the magnetic field in the study and the resulting mechanical strain fields, which were applied to the sample for moving the nanoparticles in the sample.

Kasai's autocorrelation velocity estimation method was used for determining the optical Doppler velocity.[34] According to the Kasai autocorrelation velocity estimation method, when a broadband light beam is incident on a flowing fluid, reflection can occur due to the presence of floating solid particles or air bubbles with velocity that is approximately similar to the fluid velocity.[35] The Doppler frequency shift induced by a moving particle can be expressed as $F_D = \Delta\phi/2\pi t$, where t is the time between successive A-scans and $\Delta\phi$ is the mean phase change. The Doppler frequency shift is continuously observed

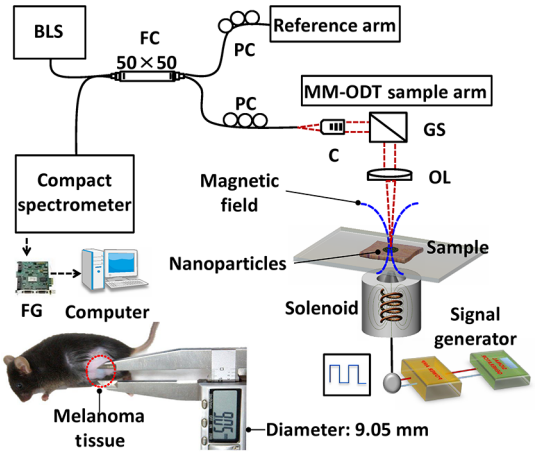

Fig. 1 Schematic of the MM-ODT experimental setup. BLS, broadband laser source; C, collimator; FC, fiber coupler; FG, frame grabber; GS, galvano-scanner; OL, objective lens; and PC, polarization controller.

during the magnetic activation. The Doppler flow velocity $\vec{V}$ can be expressed as $V = \lambda_0 f_D/2n\cos(\theta)$, where λ_0 is the center wavelength, n is the refractive index, and θ is the angle between the flow and probe beam direction (the Doppler angle).

Moreover, an iron core solenoid coil (470 turns, 2.6 Ω impedance) with a cone-shaped ferrite core was placed below the sample to provide a magnetic flux toward the entire area of the sample during MM-ODT imaging, for moving the nanoparticles in the sample. A waveform generator (Agilent, 33220A) was used for applying the magnetic field. The magnetic field intensity was dramatically increased by using the high-power combination; the magnetic field intensity was $B_{\max} = 1$ T and $\Delta|B|^2 = 220$ T^2/m at the tip of the core toward the targeted sample. Note that in this experiment, the maximal magnetic flux density (0.5596 T) was measured when the solenoid core was at a distance of 5 mm from the sample. However, due to the limitations of the experimental setup, the sample had to be kept at a distance of 10 mm from the solenoid core and the measured flux density at this stage was ~0.33077 T.

Instead of using a lock-in method-based sinusoidal magnetic force, a continuously modulating 5-Hz square wave magnetic actuation frequency with a maximal voltage of 90 V_{p-p} was applied for generating the magnetic force to achieve distinguishable Doppler signals. For the maximal distinguishable detection capability of SPIO nanoparticles, the magnetic actuation frequency was set to 5 Hz to avoid reducing the magnetic actuation duty cycle below the rising time of the iron core solenoid, which would barricade the magnetic flux intensity from reaching its maximal value, according to the slew rate theorem.

Unlike the other conventional magneto-motive systems, the lateral components of the magnetic field are negligible and a concentrated magnetic field, which is dominant in axial direction applied toward the imaging region that minimizes the negative effects of the nonuniform spatial distribution of magnetic fields. Thus, the displacement of the nanoparticles in this experiment was primarily in the axial direction.

2.2 *Preparation of the Superparamagnetic Iron Oxide Nanoparticles Injected into Ex Vivo and In Vivo Samples*

Commercially available SPIO magnetic nanoparticles were used as the contrast agents in this experiment. To observe the Doppler

shifts in the tissue samples, we prepared a solution containing nanoparticles. As an initial preparation, SPIO Ferumoxide nanoparticles (AMI-25, Guerbet Berlex Laboratories, France) with diameters in the 80- to 150-nm range were used in this experiment. The nanoparticles solution consisted of 50 ml of 5% dextrose solution and 1 ml pure Ferumoxide nanoparticles with a concentration of 0.67×1012 iron particles μl^{-1} (1.12 μg iron μl^{-1}). The prepared nanoparticles were dissolved in the glucose solution, and the solution was injected directly into a pork belly sample and an *in vivo* melanoma sample, for MM-ODT image acquisition. The experiment was repeated for different SPIO concentrations and solenoid voltage values in order to validate the system performance. Subsequently, *in vivo* melanoma skin cancer tissue was imaged to determine the performance of the MM-ODT system. The used animal model was a mouse (42- to 48-days old, 23 to 26 g) with an immune deficiency. The animal experiments were performed in accordance with the guidelines of the Institutional Animal Care and Use Committee of Kyungpook National University. Melanoma cells were transplanted into the hind leg skin of the mouse, which caused an externally visible solid tumor (5 to 9 mm). The transplanted melanoma cells were grown rapidly, in a short cancer cell growth cycle, as a result of the immune deficiency of the mouse.

2.3 *Implementation of Signal Processing for Magneto-Motive Optical Doppler Tomography*

A compute unified device architecture (CUDA)-activated digital signal processing technique was implemented for enhancing the acquisition speed in MM-ODT measurements. Figure 2 shows the flowchart, demonstrating the data path, the thread events, and the buffering for the CUDA-activated MM-ODT system. First, the data acquisition thread stored incoming two-dimensional (2-D) raw signals in the first buffer allocated in the host memory and called the signal processing thread.

Then, the self-iterated acquisition thread continually transferred the incoming signals into the second buffer without any temporal delay between adjacent acquisition events. The signal processing thread copied the frame data stored in the buffers of the host memory. *k*-domain linearization was completed by using full-range *k*-domain linearization.[36] The reconstructed MM-ODT images were transferred back to the host memory for displaying. Therefore, the frame rate of the utilized spectral domain optical coherence tomography system was increased by employing this rapid image processing procedure.

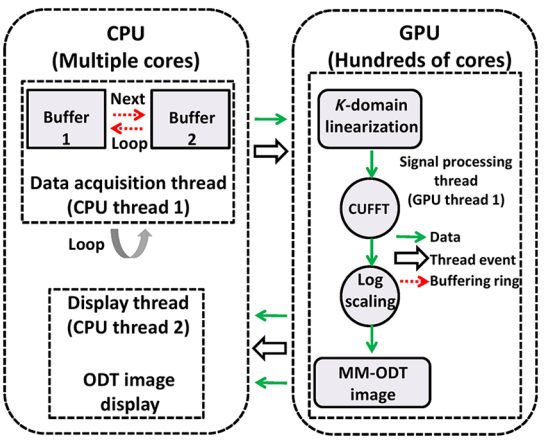

Fig. 2 CUDA-activated signal processing.

3 Results and Discussion

3.1 *Ex Vivo Magneto-Motive Optical Doppler Tomography Imaging of Pork Belly Sample*

Prior to performing the *in vivo* validation, we investigated the efficacy of the proposed system with respect to an *ex vivo* pork belly sample implanted with nanoparticles. The motion of the implanted nanoparticles was barely observable in the corresponding B-mode images of MM-OCT and MM-ODT [Figs. 3(a) and 3(b)]. The magenta-colored MM-ODT signals were overlaid on the blue-colored MM-ODT signals, making it difficult to precisely determine the nanoparticles motion. One of the reasons for the color variation was the frequency mismatch between the galvano-scanner frequency and the magnetic flux frequency. Consequently, the galvano-scanned part of the sample failed to experience the maximal magnetic force in the consistent and timely manner. Therefore, for a better identification, M-mode images consisting of 780×500 pixels axially and temporally were acquired and are shown in Figs. 3(c) and 3(d). The nanoparticles motion was clearly and continuously observed in both the MM-OCT and MM-ODT M-mode images. However, the absence of the galvano-scanner motion yielded a stronger enhancement of the periodically varying MM-ODT M-Mode signal, compared with the MM-OCT M-mode signal.

Figure 4 shows the quantitative evaluation of the average Doppler velocities as a function of the SPIO nanoparticles concentration and the applied solenoid voltage. Closed circles and dashed lines denote the measured values and the linear fitting results, respectively. Note that the experiment was repeated five consecutive times. The error bars illustrate the fluctuation range between the obtained minimum and the maximum Doppler velocity values for each corresponding concentration and induced voltage values. The linear regression represents the general tendency of linearly increasing averaged Doppler velocity values. The initially applied concentrations were 0.5, 1.0, 1.5, and 2.0 mg/ml and the injected volume was 100 μl. Second, the solenoid voltage was varied between 0 and 90 V_{p-p} with an SPIO concentration of 2.0 mg/ml [Fig. 4(b)]. The experimental Doppler velocity data were calculated by

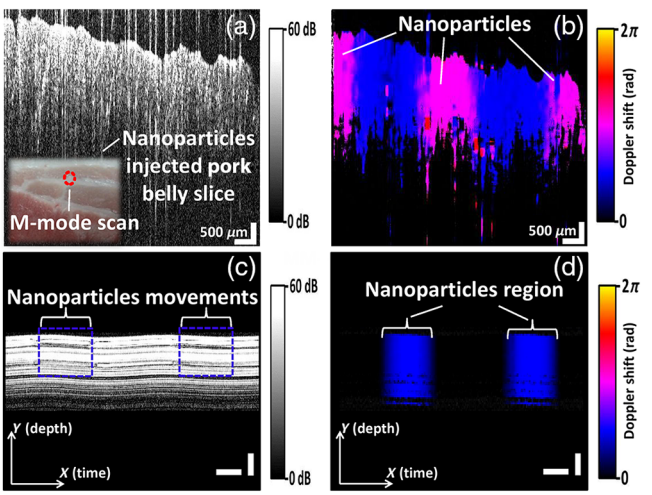

Fig. 3 MM-OCT and MM-ODT images of SPIO nanoparticles injected into the *ex vivo* pork belly sample. (a) MM-OCT image, (b) MM-ODT image with Doppler signals, (c) MM-OCT M-mode image, and (d) MM-ODT M-mode image with identifiable Doppler signals. White vertical bar: 500 μm and white horizontal bar: 20 ms.

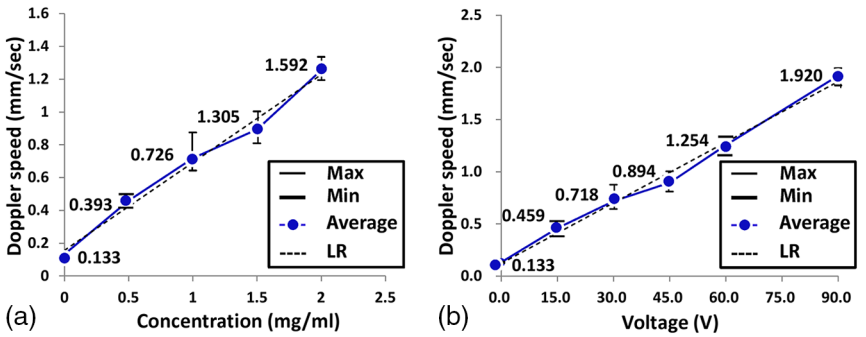

Fig. 4 Average measured Doppler velocity versus the (a) SPIO nanoparticles concentration and (b) the solenoid voltage. LR, linear regression. The error bars represent the fluctuation between the minimum and the maximum values.

using the Kasai autocorrelation velocity equations [Eqs. (1) and (2)].[35] As expected, the measured average Doppler velocity increased with increasing the nanoparticles concentration and with increasing the applied solenoid voltage.

3.2 *Histological Comparison of Melanoma Tissue Samples With and Without Injected Nanoparticles*

Prior to the MM-ODT image acquisition, histological analysis was conducted to confirm the existence of melanoma cells and magnetic nanoparticles. Hematoxylin and eosin (H&E) dye reagent was used for identifying melanoma cells, and Prussian blue dye reagent was used for identifying magnetic nanoparticles. Figure 5(a) shows the H&E-treated melanoma tissue and Fig. 5(b) shows the magnified view of the dashed rectangular area in Fig. 5(a). The H&E reagent is the most commonly used histological staining reagent and it contains an acidic dye, eosin, and a basic dye, hematoxylin. It stains melanin structures in purplish blue. The left portion of the tissue region in Fig. 5(b) has a purplish blue stain owing to a high melanin pigment content characteristic of melanoma cells, while the right portion of that same tissue region has a very slight purple stain, owing to a low melanin pigment content. Hence, the H&E control experiment confirmed the presence of melanoma cells. Melanoma tissues treated by the Prussian blue reagent were used for identifying the implanted nanoparticles, as shown in Figs. 5(c) and 5(d). Prussian blue is a dark blue pigment with the idealized formula $Fe_7(CN)_{18}$ and it is not soluble in water. The Prussian blue reaction involves treating sections with acid solutions of ferrocyanides. If any ferric ions are present in the tissue, they combine with the ferrocyanides, forming a bright blue stain. A negative staining response is observable in Figs. 5(c) and 5(d), stemming from the absence of iron particles.

We repeated the above experiment under the same experimental conditions for the melanoma tissue sample into which nanoparticles were injected, for confirming the molecular interaction between the melanoma cells and the injected magnetic nanoparticles. The dashed ellipses in Figs. 5(e) and 5(f) indicate blood vessels, which were identified after applying the H&E reagent. The purplish blue color around the blood vessels indicates the presence of live melanoma cells. The brownish regions surrounding the melanoma cells represent the injected nanoparticles.

In Figs. 5(g) and 5(h), the melanoma tissue regions are surrounded by dark blue boundaries as a result of the reaction between the SPIO magnetic nanoparticles and the Prussian blue reagent. Therefore, Figs. 5(g) and 5(h) confirm the molecular interaction between the melanoma cells and the magnetic nanoparticles, manifested as an obvious variation of color, because it verifies the applicability of MM-ODT signals to detecting particular melanoma regions.

3.3 *In Vivo Magneto-Motive Optical Doppler Tomography Imaging of Melanoma Tissue*

To gain a better understanding of the process, we performed *in vivo* imaging of a mouse skin that did not contain nanoparticles. As shown in Fig. 6(a), red-colored MM-ODT signals were obtained with a noise region as a result of the animal body motion during breathing. Second, nanoparticles (concentration

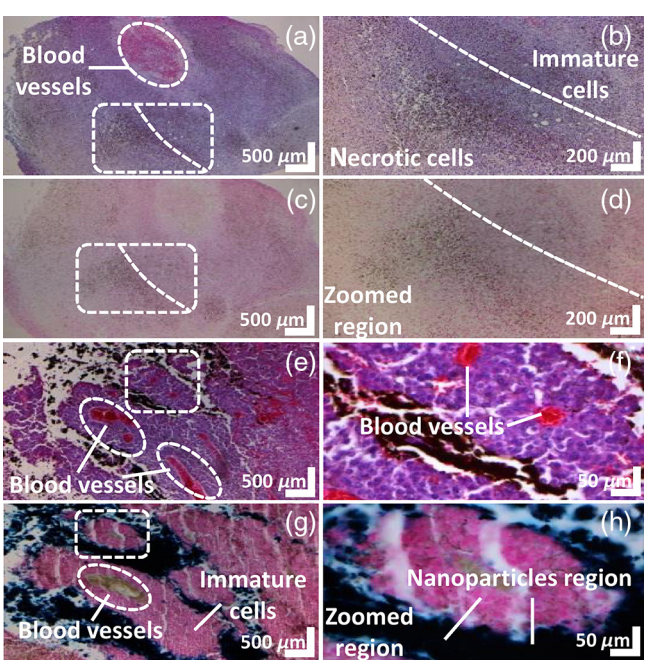

Fig. 5 Histological images of the mouse skin tissue with and without nanoparticles injection. (a) H&E-treated melanoma tissue without nanoparticles, (b) a magnified view of the dashed rectangular region in (a), (c) Prussian-blue-treated melanoma tissue without nanoparticles, (d) a magnified view of the dashed rectangular region in (c), (e) H&E-treated melanoma tissue with nanoparticles injected into it, (f) a magnified view of the dashed rectangular region in (e), (g) Prussian-blue-treated melanoma tissue with nanoparticles injected into it, and (h) a magnified view of the dashed rectangular region in (g).

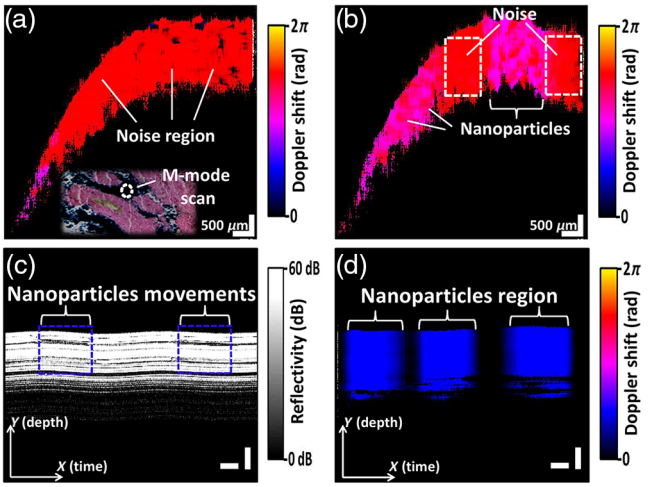

Fig. 6 MM-OCT and MM-ODT images of *in vivo* melanoma tissue. (a) An MM-ODT 2-D image of melanoma tissue without nanoparticles, (b) an MM-ODT 2-D image of melanoma tissue with nanoparticles injected, (c) an MM-OCT M-mode image of melanoma tissue with injected nanoparticles showing the Doppler shift variation for the nanoparticles, and (d) an MM-ODT M-mode image of melanoma tissue with injected nanoparticles showing the color change in the Doppler signal. White vertical bars: 500 μm and white horizontal bars: 20 ms.

of 15 mg/ml) were injected into the mouse skin for characterizing the necessity of the contrast agents. Figure 6(b) shows the results of this experiment. Although the Doppler signals owing to the motion of the injected nanoparticles were identified (magenta color), the noise region was observed as well. Limited frame acquisition speed, frequency mismatch, and motion of the mouse body during breathing can be considered as the main causes underlying the appearance of this noise.

The effect of these limitations was removed by performing the M-mode analysis. Doppler shift variations associated with the injected nanoparticles were observed in the MM-OCT image [Fig. 6(c)]. Subsequently, a dramatic reduction in the intensity of noise signals and optimal Doppler signals (blue-colored Doppler signals) in response to the periodically applied magnetic force can be identified in Fig. 6(d) throughout the area of 780×500 pixels in the axial and temporal dimensions, respectively. This result is of sufficient quality to allow us to conclude that the MM-ODT M-mode images yield more detailed information on the Doppler shift compared with the B-mode images. Therefore, MM-ODT M-mode images are more versatile for detecting melanoma tissue.

As before, we measured the average Doppler velocity for different SPIO nanoparticle concentrations and different values of the induced solenoid voltage. The concentrations that we considered were 0, 5, 10, and 15 mg/ml. A volume of 100 μl from each diluted solution was injected into the melanoma lesion and held for 20 min before acquiring the corresponding MM-ODT image. Due to the volume of the melanoma tissue region (9.05 mm $\times$ 4.23 mm $\times$ 2.00 mm), 100μl of SPIO nanoparticles solution had to be injected to obtain a sufficient distribution of nanoparticles homogeneously even though the tissue swelled slightly. The dependence of the average Doppler velocity on the induced solenoid voltage was examined by increasing the voltage from 11.25 to 90 V_{p-p}, in steps of 11.25 V. In these experiments, the concentration of the injected SPIO nanoparticles was 15 mg/ml, and the injected volume was 100 μl. Each concentration and voltage experiment was repeated five times, and the average values are plotted in Figs. 7(a) and 7(b). Similar to the previous demonstration, these results confirmed that the Doppler velocity can be increased by increasing both the applied solenoid voltage and the SPIO nanoparticles concentration.

4 Conclusion

Herein, we demonstrated an initial experiment for validating the ability of MM-ODT to identify SPIO nanoparticles implanted *in vivo* melanoma cells. The Doppler velocity was measured by utilizing the Kasai algorithm, and it was confirmed that the optical Doppler velocity is directly proportional to the concentration of the SPIO solution and the voltage applied to the solenoid. The versatility of the system was demonstrated by analyzing its ability to detect biosignals from melanoma tissue. The results of this study confirm the MM-ODT system as an effective tool for *in vivo* imaging that allows observation of living tissue implanted with magnetic nanoparticles. Thus, this method is likely to be of importance in the clinical setting for melanoma detection, even when no fluid flow is observed in the analyzed tissue. As a future extension of this study, biotargeting agents-based SPIO magnetic nanoparticles will be systematically injected into the blood vessels to enhance the accuracy and the promising capability of the method.

Acknowledgments

The authors are grateful to the Industrial Strategic Technology Development Program, Grant No. 10047943 and the

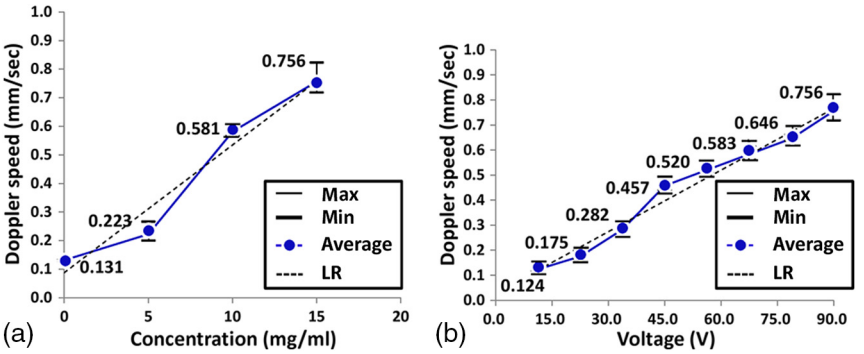

Fig. 7 Average Doppler velocity versus (a) the SPIO nanoparticles concentration and (b) the applied voltage. LR, linear regression. The error bars represent the fluctuation between the minimum and the maximum values.

"Development of MicroSurgical Apparatus Based on 3-D Tomographic Operating Microscope" program, funded by the Ministry of Trade, Industry, and Energy (MI, Korea, No. 10047943). This study was also supported by the BK21 Plus project funded by the Ministry of Education, Korea (No. 21A20131600011).

References

1. C. M. Balch et al., "Final version of 2009 AJCC melanoma staging and classification," *J. Clin. Oncol.* **27**(36), 6199–6206 (2009).
2. V. Nikolaou and A. Stratigos, "Emerging trends in the epidemiology of melanoma," *Br. J. Dermatol.* **170**(1), 11–19 (2014).
3. I. Anteby and J. Pe'er, "Ultrasonography—a major imaging tool in the diagnosis of intraocular tumors," *Harefuah* **124**(2), 96 (1993).
4. S. F. Byrne and R. L. Green, *Ultrasound of the Eye and Orbit*, Mosby-Year Book, Inc., St. Louis (1992).
5. V. Cohen et al., "Transvitreal fine needle aspiration biopsy: the influence of intraocular lesion size on diagnostic biopsy result," *Eye* **15**(2), 143–147 (2001).
6. D. Huang et al., "Optical coherence tomography," *Science* **254**(5035), 1178–1181 (1991).
7. W. Jung et al., "Handheld optical coherence tomography scanner for primary care diagnostics," *IEEE Trans. Biomed. Eng.* **58**(3), 741–744 (2011).
8. N. H. Cho et al., "Development of real-time dual-display handheld and bench-top hybrid-mode SD-OCTs," *Sensors* **14**(2), 2171–2181 (2014).
9. T. Gambichler et al., "Applications of optical coherence tomography in dermatology," *J. Dermatol. Sci.* **40**(2), 85–94 (2005).
10. P. Lenton et al., "Imaging in vivo secondary caries and ex vivo dental biofilms using cross-polarization optical coherence tomography," *Dent. Mater.* **28**(7), 792–800 (2012).
11. N. H. Cho et al., "In vivo imaging of middle-ear and inner-ear microstructures of a mouse guided by SD-OCT combined with a surgical microscope," *Opt. Express* **22**(8), 8985–8995 (2014).
12. X. Wang, T. Milner, and J. Nelson, "Characterization of fluid flow velocity by optical Doppler tomography," *Opt. Lett.* **20**(11), 1337–1339 (1995).
13. Z. Chen et al., "Optical Doppler tomographic imaging of fluid flow velocity in highly scattering media," *Opt. Lett.* **22**(1), 64–66 (1997).
14. Z. Chen et al., "Optical Doppler tomography," *IEEE J. Select. Topics Quantum Electron.* **5**(4), 1134–1142 (1999).
15. R. Aaslid, T.-M. Markwalder, and H. Nornes, "Noninvasive transcranial Doppler ultrasound recording of flow velocity in basal cerebral arteries," *J. Neurosurg.* **57**(6), 769–774 (1982).
16. H. Wehbe et al., "Automatic retinal blood flow calculation using spectral domain optical coherence tomography," *Opt. Express* **15**(23), 15193–15206 (2007).
17. D. M. Bukowska et al., "Assessment of the flow velocity of blood cells in a microfluidic device using joint spectral and time domain optical coherence tomography," *Opt. Express* **21**(20), 24025–24038 (2013).
18. Y. Zhao et al., "Doppler standard deviation imaging for clinical monitoring of in vivo human skin blood flow," *Opt. Lett.* **25**(18), 1358–1360 (2000).
19. A. L. Oldenburg et al., "Phase-resolved magnetomotive OCT for imaging nanomolar concentrations of magnetic nanoparticles in tissues," *Opt. Express* **16**(15), 11525–11539 (2008).
20. A. Oldenburg et al., "Magnetomotive contrast for in vivo optical coherence tomography," *Opt. Express* **13**(17), 6597–6614 (2005).
21. X. Huang et al., "Cancer cell imaging and photothermal therapy in the near-infrared region by using gold nanorods," *J. Am. Chem. Soc.* **128**(6), 2115–2120 (2006).
22. X. Liu et al., "Au-Cu2–x Se heterodimer nanoparticles with broad localized surface plasmon resonance as contrast agents for deep tissue imaging," *Nano Lett.* **13**(9), 4333–4339 (2013).
23. I. J. M. de Vries et al., "Magnetic resonance tracking of dendritic cells in melanoma patients for monitoring of cellular therapy," *Nat. Biotechnol.* **23**(11), 1407–1413 (2005).
24. J. Pintaske et al., "Effect of concentration of SH U 555A labeled human melanoma cells on MR spin echo and gradient echo signal decay at 0.2, 1.5, and 3T," *Magn. Reson. Mater. Phys. Biol. Med.* **19**(2), 71–77 (2006).
25. D. Spira et al., "Labeling human melanoma cells with SPIO in vitro observations," *Mol. Imaging* **15**, 1–10 (2016).
26. P. Reimer et al., "SPIO-enhanced 2D-TOF MR angiography of the portal venous system: results of an intraindividual comparison," *J. Magn. Reson. Imaging* **7**(6), 945–949 (1997).
27. P. Reimer and B. Tombach, "Hepatic MRI with SPIO: detection and characterization of focal liver lesions," *Eur. Radiol.* **8**(7), 1198–1204 (1998).
28. S. Schmitz et al., "Quantitative assessment of iron-oxide-enhanced magnetic resonance imaging of the liver: vessel isointensity is a potential characteristic of liver hemangiomas on late T1-weighted images," *Acta Radiol.* **47**(7), 634–642 (2006).
29. A. L. Oldenburg et al., "Spectral-domain magnetomotive OCT imaging of magnetic nanoparticle biodistribution," *Proc. SPIE* **6847**, 684719 (2008).
30. J. Kim et al., "Imaging nanoparticle flow using magneto-motive optical Doppler tomography," *Nanotechnology* **18**(3), 035504–035509 (2007).
31. J.-H. Kim and J.-H. Oh, "Nanoparticle contrast in magneto-motive optical Doppler tomography," *J. Opt. Soc. Korea* **10**(3), 99–104 (2006).
32. A. L. Oldenburg, J. R. Gunther, and S. A. Boppart, "Imaging magnetically labeled cells with magnetomotive optical coherence tomography," *Opt. Lett.* **30**(7), 747–749 (2005).
33. J. Kim et al., "Hemoglobin contrast in magnetomotive optical Doppler tomography," *Opt. Lett.* **31**(6), 778–780 (2006).
34. V. X. Yang et al., "Improved phase-resolved optical Doppler tomography using the Kasai velocity estimator and histogram segmentation," *Opt. Commun.* **208**(4), 209–214 (2002).
35. V. Yang et al., "High speed, wide velocity dynamic range Doppler optical coherence tomography (part I): system design, signal processing, and performance," *Opt. Express* **11**(7), 794–809 (2003).
36. M. Jeon et al., "Full-range k-domain linearization in spectral-domain optical coherence tomography," *Appl. Opt.* **50**(8), 1158–1163 (2011).

Mansik Jeon received his PhD in electronics engineering from Kyungpook National University, Daegu, Republic of Korea, in 2011. He is currently an assistant professor of the School of Electronics Engineering at Kyungpook National University. His research interests are in the development of nonionizing and noninvasive novel biomedical imaging techniques, including photoacoustic tomography, optical coherence tomography, ultrasonic imaging, handheld scanner, and their clinical applications.

Biographies for the other authors are not available.